

This document is downloaded from DR-NTU, Nanyang Technological University Library, Singapore.

Title	Tsunami hazard from the subduction megathrust of the South China Sea : Part I. source characterization and the resulting tsunami.
Author(s)	Megawati, Kusnowidjaja.; Shaw, Felicia.; Sieh, Kerry.; Huang, Zhenhua.; Wu, Tso-Ren.; Lin, Yunung.; Tan, Soon Keat.; Pan, Tso-Chien.
Citation	Megawati, K., Shaw, F., Sieh, K., Huang, Z., Wu, T. R., Lin, Y., et al. (2009). Tsunami hazard from the subduction megathrust of the South China Sea: Part I. source characterization and the resulting tsunami. <i>Journal of Asian Earth Sciences</i> , 36(1), 13-20.
Date	2008
URL	http://hdl.handle.net/10220/8672
Rights	© 2008 Elsevier Ltd.

Tsunami hazard from the subduction megathrust of the South China Sea: Part I. Source characterization and the resulting tsunami

Kusnowidjaja Megawati^{a,b,}, Felicia Shaw^c, Kerry Sieh^b, Zhenhua Huang^a, Tso-Ren Wu^d, Yunung Lin^e, Soon Keat Tan^a, Tso-Chien Pan^{a,c}*

^a *School of Civil and Environmental Engineering, Nanyang Technological University, 50 Nanyang Avenue, Singapore 639798, Singapore*

^b *Earth Observatory of Singapore, Nanyang Technological University, Nanyang Avenue, Singapore 639798, Singapore*

^c *Protective Technology Research Centre, School of Civil and Environmental Engineering, Nanyang Technological University, Nanyang Avenue, Singapore 639798, Singapore*

^d *Graduate Institute of Hydrological and Oceanic Sciences, National Central University, 300 Jhongda Road, Jhongli, Taoyuan, Taiwan, Republic of China*

^e *Division of Geological and Planetary Sciences, California Institute of Technology, Pasadena, CA 91125-2100, USA*

** Corresponding author. E-mail address: kusno@ntu.edu.sg (K. Megawati).*

Abstract

The subduction megathrust under the Manila Trench has been accumulating strain over a period of 440 years or more, and could be the source for a giant earthquake of $M_w \sim 9$. We present a plausible earthquake rupture model constructed from seismic and geodetic data, together with hydrodynamic simulations of the potential tsunami with COMCOT (COrnell Multi-grid COupled Tsunami model). Results indicate that this megathrust poses a risk of devastating tsunami for the Philippines, southern China, Vietnam and other population centers bordering the South China Sea.

Keywords: South China Sea megathrust, Manila trench, Tsunami Rupture model, Singapore Southeast Asia

1. Introduction

The 2004 Aceh-Andaman tsunami created unprecedented devastation to coastal communities on the rim of the Indian Ocean, killing more than 225,000 people in eleven countries and displacing over a million people. Of a similar length to the 1,500 km-long Aceh-Andaman megathrust, the active subduction zone stretching between southern Taiwan and the central west coast of the Philippines (Fig. 1) is one of the potential tsunami sources that could devastate communities bordering the South China Sea. The submarine topographic expression of the megathrust, referred to as the South China Sea megathrust hereafter, is the Manila Trench. GPS geodesy measurements show that the convergence rate across the megathrust is about 8 cm/year.

The exposure of large population centers bounding the South China Sea to tsunami hazard cannot be understated. Luzon Island, which lies just east of the Manila Trench, is the site for intensive agriculture, industry, tourism, with a number of key sea and air ports and power stations exposed to the threat of tsunami. Over eleven millions people live in the city of Manila alone, with a further 10 million people inhabiting the nine western coastal provinces. Facing the trench, Vietnam's long north-south profile renders it acutely vulnerable to tsunamis from the southern section of the megathrust (Fig. 1). Population density along the southern coast of mainland China is 100–200 people/km². Any effect to Hong Kong, one of the busiest seaports in the world and one of the main gateways to and from China, would cause significant impact to the economy of Asia and the world. Kaohsiung in southern Taiwan, the major port through which most of Taiwan's oil is imported, would paralyze economic activities in Taiwan if it were devastated by tsunami.

In this study, plausible models of earthquake rupture on the megathrust are constructed and the ensuing tsunami events are simulated using well-tested hydrodynamics model. The resulting maximum water-level rise along the coasts of the South China Sea is discussed in view to the impact on coastal communities in the

South China Sea. The possibility of a mega earthquake to occur along the trench is discussed based on historical tsunami records in southern China.

2. Regional tectonics

The Manila Trench is the 1500 km-long submarine expression of the east-dipping South China Sea subduction zone, which initiated in the early Miocene (22–25 Ma) and remains active to the present day (Fuller et al., 1983; Bellon and Yumul, 2000; Yumul et al., 2003; Queano et al., 2007). Along this subduction zone, the oceanic crust of the South China Sea descends eastward beneath the Philippines, southernmost Taiwan and the intervening ocean floor (Fig. 1). The broadly convex-westward shape of the Manila Trench is due to the westward migration of Luzon over the subducting oceanic slab, while the southern and northern ends of the trench are pinned at collisions at the latitudes of Palawan Island (~12 °N, 120 °E) and southern Taiwan (~23 °N, 120 °E) (Bautista et al., 2001).

3. Parameters of the megathrust

To characterize the South China Sea megathrust, we first considered the geometry of the potential rupture area. Between 13 °N and 22.5 °N, the distribution of trench-related earthquakes shows the dip of the subducting slab varies from less than 20 ° in the shallow part to greater than 50 ° at greater perpendicular distances (Bautista et al., 2001). Notably, the slab profile shallows considerably over the region of 20–20.5 °N. The Wadati-Benioff zone does not extend north of 23 °N, as a result of the transition from subduction of oceanic lithosphere to collisional tectonics (Shyu et al., 2005). However, *P*-velocity tomograms at 23.5 °N appear to indicate deformation of the oceanic slab beneath Taiwan (Wu et al., 2007). At the southern extremity of the megathrust, the micro-continent of Palawan is in collision with the rest of the Philippine archipelago, and the Wadati-Benioff zone is not apparent beyond 12.5 °N (Rangin et al., 1999). At these pinned ends of the megathrust, where the morphology of the down-going slab becomes indistinct, we infer steeply dipping profiles.

Fig. 2 shows the surface of the rupture model, which was obtained by interpolation

passing through ten seismic cross sections between latitude 12.5 °N and 23.5 °N from the studies by Bautista et al. (2001) and Wu et al. (2007). The nine cross sections from Bautista et al. (2001) are indicated as A–A*, B–B*, ..., I–I*, whereas the single section from Wu et al. (2007) is marked as W–W*. The upper boundary of the megathrust is naturally delineated by the Manila Trench, which reaches a depth of 4 km below sea-level and is broadly convex towards the west. Second-order irregularities in its shape appear to be due to uneven topography of the subducting oceanic slab. The trace of the Manila Trench was derived from 2 min resolution bathymetry data (ETOPO2), and thereafter smoothed using polynomial spline fitting.

The eastern, downdip extent of the rupture model was defined by the lower limit of seismicity. This appears to lie between 40 and 60 km depth, demarcating the brittle-plastic transition zone. We discriminate from earthquakes associated with internal deformation of the slab, by only considering thrust-mechanism hypocenters located close to the interpreted surface of the slab. The closeness of fit to the surface of the rupture model is illustrated in Fig. 2.

Next, we placed constraints on possible coseismic slip, via analysis of geodetic data for Luzon relative to stable Eurasia. To avoid using data contaminated by complex deformation, only GPS vectors east of the Philippine Fault Zone were considered. Yu et al. (1999) used 35 GPS stations on Luzon Island and southern Taiwan to calculate the relative motion between Luzon arc and Eurasia. The observation was conducted for two years, from 1996 to 1998. Relative motion is greatest in northern Luzon at 19 °N, moving 86–90 mm/yr northwestward. The velocities taper gradually towards the north and south as collision regimes pin both ends of the megathrust (Fig. 3).

The velocity vectors were decomposed into trench-normal and trench-parallel components (Fig. 3), allowing us to infer that the former are related to slow accumulation of strain along the plate, while the latter are accommodated by strike-slip motion across the Philippine Fault Zone and slip on other geological structures. This would be analogous to the partitioning of trench-normal and trench-parallel strain across the Sunda megathrust and the strike-slip Sumatran Fault (McCaffrey et

al., 2000).

It is significant that since the Spanish colonization of Luzon in the 1560s, no earthquake exceeding magnitude 7.8 has been observed (Repetti, 1946). Conservatively, it can be postulated that very large events on this megathrust have a recurrence interval exceeding 440 years. Taking a trench-normal convergence velocity of 87 mm/yr, strain of ~38 m would have accumulated over this period. Though large, this slip magnitude remains within the range of plausible scenarios. It is comparable to the 1960 M_w 9.5 Chilean earthquake, in which coseismic slip reached 40 m (Barrientos and Ward, 1990), and larger than the 2004 Aceh-Andaman event, which produced 20 m of coseismic slip (Chlieh et al., 2007).

In our rupture model, we set slip values in the area of greatest relative motion to 40 m, and apply the same geometric scale to the rest of the vector data points, smoothing the variation between them. Slip is taken to be constant approximately perpendicular to the trench axis. This is a necessary simplification as we have inadequate data to constrain the downdip variation in locking. Fig. 4 illustrates the projected slip model of the megathrust.

In order to find the vertical seafloor displacement for hydrodynamic modeling, the megathrust interface was discretized into 33 rectangular elements as shown in Fig. 5. Along-strike variation and the dip angle were matched closely to the continuous slip model. Two rows of elements were used, where the first row, starting from element No. 1 to 18, covers the megathrust interface from the surface up to a depth of 15 km, whereas the second row (element Nos. 19–33) covers the interface from 15 to 55 km deep. Slip magnitudes were assigned directly such that the value for each rectangular element conforms to the value at its centroid position on the continuous model. The orientation (strike and dip angles), size (length and width), and slip magnitude of each element are summarized in Table 1. This rupture model would produce an earthquake with M_w 9.0.

The thrust interface was assumed to be fully locked, i.e. the coefficient of coupling was assigned as 1. A source point was placed at the centroid of each element to simulate dislocation, and the surface deformation with that geometry was computed

using an elastic half-space dislocation algorithm (Okada, 1992). The resulting vertical seafloor deformation (Fig. 6) was sampled to 1 min (0.016 °) and 2 min (0.033 °) grid resolutions over an area within 99 °E/140 °E/10 °S/40 °N. Large uplifting of up to 9 m occurs along the trench, whereas down-going movement of up to 4 m occurs about 150 km east of the trench, mostly on Luzon Island.

4. Regional water-level rise

Tsunami generated by the rupture of the South China Sea megathrust is simulated using COMCOT (COrnell Multi-grid COupled Tsunami model), developed by Liu et al. (1998). COMCOT uses a finite difference scheme to solve linear/non-linear shallow-water equations (Wang and Liu, 2005, 2006, 2007; Gica et al., 2007). The detailed modeling of the problem and characteristics of tsunami propagation throughout the South China Sea are discussed in the companion paper (Huang et al., 2009). Here, we focus on the resulting water-level rise in the region. Water waves were propagated to within 10 m off the shore, thus no effects of inundation are considered.

Fig. 7 shows maximum simulated water-level rise at shorelines bordering the South China Sea, over 40 h of physical time. Note that they are considered to be offshore waves as we used grids with a course resolution of 2.4 min, which could not fully resolve the shoaling process (Huang et al., 2009). Naturally, the western coast of Luzon Island is the hardest hit area with waves of more than 8 m due to its proximity to the source. Waves of more than 8 m are projected to strike the islands of Batan and Babuyan (~20 °N, 122 °E) lying between the Philippines and Taiwan. The western coast of Palawan Island (~11 °N, 119.5 °E), south of Luzon Island, is hit by waves of 4 m high.

Southern China, including Hong Kong and Macau, being on the other side of the Manila Trench is exposed to tsunami waves of 6–8 m high. The focusing effects of the tsunami source and local bathymetry are oriented northwest, resulting to southern China being as badly hit as the Philippines although the former is located farther from the subduction.

The western coast of Vietnam is struck by waves of 4–5 m, showing that it is not fully shielded by the Paracel Islands (~16°N, 112°E). The western coast of Borneo receives waves of 2 to 3 m, whereas the eastern coast of Malay Peninsula is hit by waves of up to 2 m. Singapore, on the southern tip of the Malay Peninsula, is well shielded and hardly affected.

Farther in the north, Taiwan receives the impact of reflections from mainland China, and the central western coast appears to suffer waves of up to 3 m in height. The southern Japanese islands of Ishigaki, Miyako and Okinawa (~25°N, 125°E) also suffer from reflective waves and may experience waves of about 2 m. It appears that the reflective waves travel to, as far as, northern Papua (~2°S, 137°E), which may be hit by waves of up to 2 m.

5. Discussion and conclusion

The degree to which the convergence on the South China Sea megathrust is accommodated by aseismic versus seismic slip is poorly constrained. The only attempt to model the extent of the seismic coupling was carried out by Galgana et al. (2007), using a system of elastic blocks delimited by major trenches and strike-slip faults in the Philippines. Regional geodetic data and focal mechanism data were jointly inverted to derive plate rotations and fault-locking parameters for their tectonic model. They concluded that, with an assumed locking depth at 25 km, the coupling ratio of the Manila Trench was low, implying that the potential for the megathrust to generate giant earthquake was low. However, spatial resolution of the crustal model was limited by paucity of GPS data in northern Luzon (Galgana et al., 2007), and results for the Manila Trench were dependent on the stability of the entire modeled system. This means that large uncertainty still exists on the actual coupling on the mega-thrust. Therefore, there is a need for increased coverage in future geodetic surveys, particularly in northern Luzon. The presence of the strike-slip Philippine Fault Zone and secondary tectonic structures should be taken into account. The Luzon Strait between 18°N and 22°N is currently void of data. Ocean-bottom seismometry and geodesy are vital in tracking the dynamics of deformation

offshore.

The South China Sea megathrust would be the first suspect source for any large historical tsunamis on the shores of the South China Sea. Observations of natural phenomena in China begin from as early as 47 B.C., and the Philippine record begins in 1589 A.D., some time after the archipelago came under Spanish colonial rule. We find that two events are of particular significance. These are marked in Fig. 1, along with significant tsunamis mapped on the west coast of Luzon (Besana et al., 2005).

The first possible megathrust tsunami dates from 1076 A.D. Official Chinese records describe flooding of the cities of Haiyang and Chaoyang (on the mainland, east and west of modern-day Hong Kong). The intervening area was sparsely populated, but some 500 km of coastline may have been flooded (Yang and Wei, 2005). If caused by tectonic activity, the earthquake that caused it would have been huge, and its likely source could have been the South China Sea megathrust. Unfortunately, the 1076 event pre-dates the Philippine record.

The second suspected tsunami inundated Kaohsiung, southwestern Taiwan, in 1781 (Wang et al., 2006). Besides appearing in a contemporary Chinese travelogue and a Japanese historiography, it was also recorded by Dutch colonists in the 18th-century Taiwan. Flooding lasted upwards of 8 h and many villages were swept away, resulting in more than 40,000 casualties (Wang et al., 2006). Despite the severity of this event, no inland or near-shore earthquake was identified as the cause. This would be consistent with the theory that the tsunami was generated by a far-field earthquake from off the Philippines.

The identification of palaeotsunami deposits on the coastlines of the Philippines, southern China and Vietnam would place constraints on pre-historic activity of the megathrust. Suspected tsunami events in the region require correlation with as many lines of evidence as possible. There is a strong case for renewed examination of extant historical documents, which may reveal the magnitude and frequency of hitherto unknown events.

The segmentation of the South China Sea megathrust is currently an area of active research. Earthquake hypocenters cluster in the area where the Scarborough Sea Mounts are being subducted under Luzon (at $\sim 16.5^{\circ}\text{N}$). These sea mounts may act as asperities, changing the nature of rupture propagation at this juncture.

The rupture model may thus be qualitatively subdivided into northern and southern segments, with the hinge point at $\sim 16.5^{\circ}\text{N}$. In these instances, different focusing effects of the tsunami would arise, due to the sinuosity of the rupture model. If the northern segment ruptures, the tsunami would be directed towards southern China, with an impact not be much lower than for the full-rupture scenario. If rupture takes place along the southern segment, the tsunami would be directed towards Vietnam and the rest of Southeast Asia.

For now, the South China Sea megathrust presents the serious possibility of a catastrophic tsunami and every effort must be made to refine our understanding of it.

Acknowledgements

This work is funded by the National Environmental Agency, Singapore. The opinions described in this paper are of the authors and may not necessarily reflect the standing of the funding agency. The authors would also like to thank Professor Philip L.-F. Liu of Cornell University for providing the latest version of COMCOT used in the present study and also for coordinating this special issue. This is Contribution No. 2 of Earth Observatory of Singapore at Nanyang Technological University.

References

- Barrientos, S.E., Ward, S.N., 1990. The 1960 Chile earthquake – inversion for slip distribution from surface deformation. *Geophysical Journal International* 103, 589–598.
- Bautista, C.B., Bautista, M.L.P., Oike, K., Wu, F.T., Punongbayan, R.S., 2001. A new insight on the geometry of subducting slabs in northern Luzon, Philippines. *Tectonophysics* 339, 279–310.
- Bellon, H., Yumul, G.P., 2000. Mio-Pliocene magmatism in the Baguio Mining District (Luzon, Philippines): age clues to its geodynamic setting. *Comptes Rendus De L Academie Des Sciences Serie II Fascicule A-Sciences De La Terre Et Des Planetes* 331, 295–302.
- Besana, G.M., Ando, M., Mirabueno, H., Daligdig, J.A., Abigania, M.I.T., Amilbahar, R., Panol, M., de La Cruz, L., del Rosario, R., Solidum, R.U., Tanioka, Y., 2005. Tsunamis in the Philippines: mapping and Assessment in the Last Five Years. In: *Workshop on Tsunami Deposits and Their Role in Hazards Mitigation*.
- Chlieh, M., Avouac, J.-P., Hjorleifsdottir, V., Song, T.-R.A., Ji, C., Sieh, K., Sladen, A., Hebert, H., Prawirodirdjo, L., Bock, Y., Galetzka, J., 2007. Coseismic slip and afterslip of the great M_w 9.15 Sumatra-Andaman earthquake of 2004. *Bulletin of the Seismological Society of America* 97, S152–S173.
- Fuller, M., McCabe, R., Williams, S., Almasco, J., Encina, R.Y., Zanoria, A.S., 1983. Paleomagnetism of Luzon. In: Hayes, D.E. (Ed.), *The Tectonic and Geologic Evolution of South-East Asian Seas and Islands, Part II. Geophysics Monogram Series*, vol. 27. AGU, Washington D.C., pp. 79–94.
- Galgana, G., Hamburger, M., McCaffrey, R., Corpuz, E., Chen, Q.Z., 2007. Analysis of crustal deformation in Luzon, Philippines using geodetic observations and earthquake focal mechanisms. *Tectonophysics* 432, 63–87.
- Gica, E., Teng, M.H., Liu, P.L.F., Titov, V., Zhou, H.Q., 2007. Sensitivity analysis of

source parameters for earthquake-generated distant tsunamis. *Journal of Waterway, Port, Coastal and Ocean Engineering-ASCE* 133, 429–441.

Huang, Z., Wu, T.R., Tan, S.K., Megawati, K., Shaw, F., Liu, X., Pan, T.C., 2009. Tsunami hazard from the subduction megathrust of the South China Sea: Part II. Hydrodynamics modeling and possible impact on Singapore. *Journal of Asian Earth Sciences* 36 (1), 93–97.

Liu, P.L.F., Woo, S.B., Cho, Y.S., 1998. *Computer Programs for Tsunami Propagation and Inundation*. Cornell University.

McCaffrey, R., Zwick, P.C., Bock, Y., Prawirodirdjo, L., Genrich, J.F., Stevens, C.W., Puntodewo, S.S.O., Subarya, C., 2000. Strain partitioning during oblique plate convergence in northern Sumatra: geodetic and seismologic constraints and numerical modeling. *Journal of Geophysical Research-Solid Earth* 105, 28363–28376.

Okada, Y., 1992. Internal deformation due to shear and tensile faults in a half-space. *Bulletin of the Seismological Society of America* 82, 1018–1040.

Queano, K.L., Ali, J.R., Milsom, J., Aitchison, J.C., Pubellier, M., 2007. North Luzon and the Philippine Sea plate motion model: insights following paleomagnetic, structural, and age-dating investigations. *Journal of Geophysical Research-Solid Earth* 112 (B05101).

Rangin, C., Spakman, W., Pubellier, M., Bijwaard, H., 1999. Tomographic and geological constraints on subduction along the eastern Sundaland continental margin (South-East Asia). *Bulletin De La Societe Geologique De France* 170, 775–788.

Repetti, W.C., 1946. Catalogue of Philippine earthquakes, 1589–1899. *Bulletin of the Seismological Society of America* 36, 133–322.

Shyu, J.B.H., Sieh, K., Chen, Y.G., Liu, C.S., 2005. Neotectonic architecture of Taiwan and its implications for future large earthquakes. *Journal of Geophysical*

Research-Solid Earth 110 (B08402).

Wang, X.M., Liu, P.L.F., 2005. A numerical investigation of Boumerdes-Zemmouri (Algeria) earthquake and tsunami. *Computer Modeling in Engineering and Sciences* 10, 171–183.

Wang, X.M., Liu, P.L.F., 2006. An analysis of 2004 Sumatra earthquake fault plane mechanisms and Indian Ocean tsunami. *Journal of Hydraulic Research* 44, 147– 154.

Wang, X.M., Liu, P.L.F., 2007. Numerical simulations of the 2004 Indian Ocean tsunamis - Coastal effects. *Journal of Earthquake and Tsunami* 1, 273–297.

Wang, X.Q., Lu, J.X., Ding, X., 2006. A preliminary study on the risk of tsunami in China. *South China Journal of Seismology* 26, 76–80 (in Chinese with English abstract).

Wu, Y.M., Chang, C.H., Zhao, L., Shyu, J.B.H., Chen, Y.G., Sieh, K., Avouac, J.P., 2007. Seismic tomography of Taiwan: improved constraints from a dense network of strong motion stations. *Journal of Geophysical Research-Solid Earth* 112 (B08312).

Yang, M.L., Wei, B.L., 2005. The potential seismic tsunami risk in South China Sea and its surrounding region. *Journal of Catastrophology* 20, 41–47 (in Chinese with English abstract).

Yu, S.B., Kuo, L.C., Punongbayan, R.S., Ramos, E.G., 1999. GPS observation of crustal deformation in the Taiwan-Luzon region. *Geophysical Research Letters* 26, 923– 926.

Yumul, G.P., Dimalanta, C.B., Tamayo, R.A., Maury, R.C., 2003. Collision, subduction and accretion events in the Philippines: a synthesis. *Island Arc* 12, 77–91.

List of Table

Table 1 The orientation (strike and dip angles), size (length and width), and slip magnitude of each subfault of the South China Sea megathrust.

List of Figures

- Figure 1 The South China Sea megathrust, together with population centers bordering the sea and areas affected in historical tsunami events.
- Figure 2 The sinuous rupture interface of the South China Sea megathrust, together with ten seismic cross sections between latitude 12.5 °N and 23.5 °N from the studies by Bautista et al. (2001) and Wu et al. (2007). Epicenters of thrust-faulting earthquakes are plotted to mark the downdip boundary of the rupture interface.
- Figure 3 GPS data (Yu et al., 1999) indicating motion of the converging Eurasian plate and the Philippines Sea plate, where the blue arrows and numbers show raw velocity values (mm/yr) taken from Yu et al. (1999), the red arrow and numbers indicate velocity values (mm/yr) resolved in the direction perpendicular to the trench front, and the black numbers give the rounded values (mm/yr) used for slip estimation.
- Figure 4 The resulting slip model, where the color bar indicates slip in meters.
- Figure 5 The discretized model for computation of seafloor displacement.
- Figure 6 The resulting vertical seafloor displacement.
- Figure 7 The maximum water-level rise.

Table 1

Element No.	Strike (°)	Dip (°)	Rake (°)	Depth range (km)	Length (km)	Width (km)	Slip (km)
1	324.46	21.78	90	0-15	40.41	19.30	5
2	325.20	11.26	90	0-15	54.19	38.68	5
3	318.66	6.55	90	0-15	54.09	66.93	12
4	332.40	5.79	90	0-15	54.00	75.68	12
5	0.26	6.47	90	0-15	53.89	67.52	25
6	7.39	11.50	90	0-15	80.59	37.51	28
7	5.85	10.01	90	0-15	53.56	43.13	28
8	355.99	8.46	90	0-15	53.43	51.06	28
9	358.34	7.18	90	0-15	53.28	60.09	30
10	2.50	6.16	90	0-15	53.14	69.93	30
11	16.26	6.52	90	0-15	52.99	65.93	35
12	40.34	5.93	90	0-15	105.57	72.15	40
13	35.93	5.36	90	0-15	52.60	79.67	40
14	21.46	5.70	90	0-15	78.62	74.61	35
15	352.23	3.28	90	0-15	78.24	129.36	30
16	332.43	6.25	90	0-15	103.81	67.36	25
17	339.52	7.62	90	0-15	51.68	54.86	12
18	341.26	9.89	90	0-15	46.82	41.97	5
19	326.63	28.87	90	15-55	37.50	37.27	5
20	351.15	25.45	90	15-55	54.14	43.11	5
21	333.50	30.86	90	15-55	134.88	34.22	12
22	357.94	20.98	90	15-55	53.76	53.11	28
23	11.30	24.22	90	15-55	133.84	45.09	28
24	9.30	18.22	90	15-55	53.29	61.36	28
25	10.90	15.85	90	15-55	53.15	70.96	30
26	47.78	12.76	90	15-55	105.90	88.63	40
27	30.91	14.73	90	15-55	131.68	75.92	40
28	37.06	16.31	90	15-55	52.41	67.88	35
29	24.75	23.79	90	15-55	104.39	44.85	30
30	302.02	31.89	90	15-55	51.99	31.66	25
31	340.64	19.63	90	15-55	103.67	55.05	25
32	320.54	16.07	90	15-55	77.33	67.83	12
33	326.04	24.96	90	15-55	21.26	41.86	5

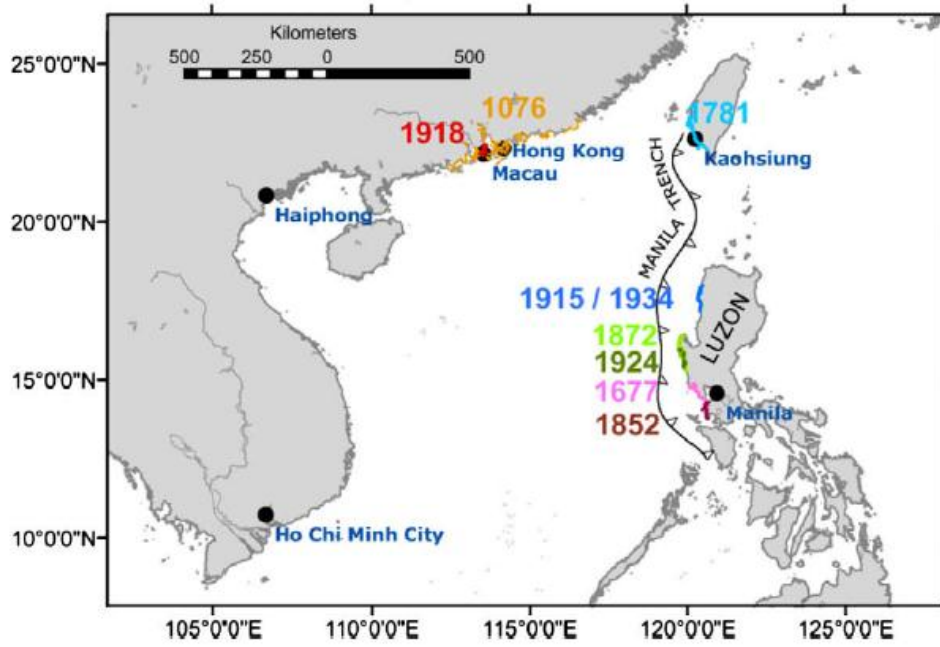


Figure 1

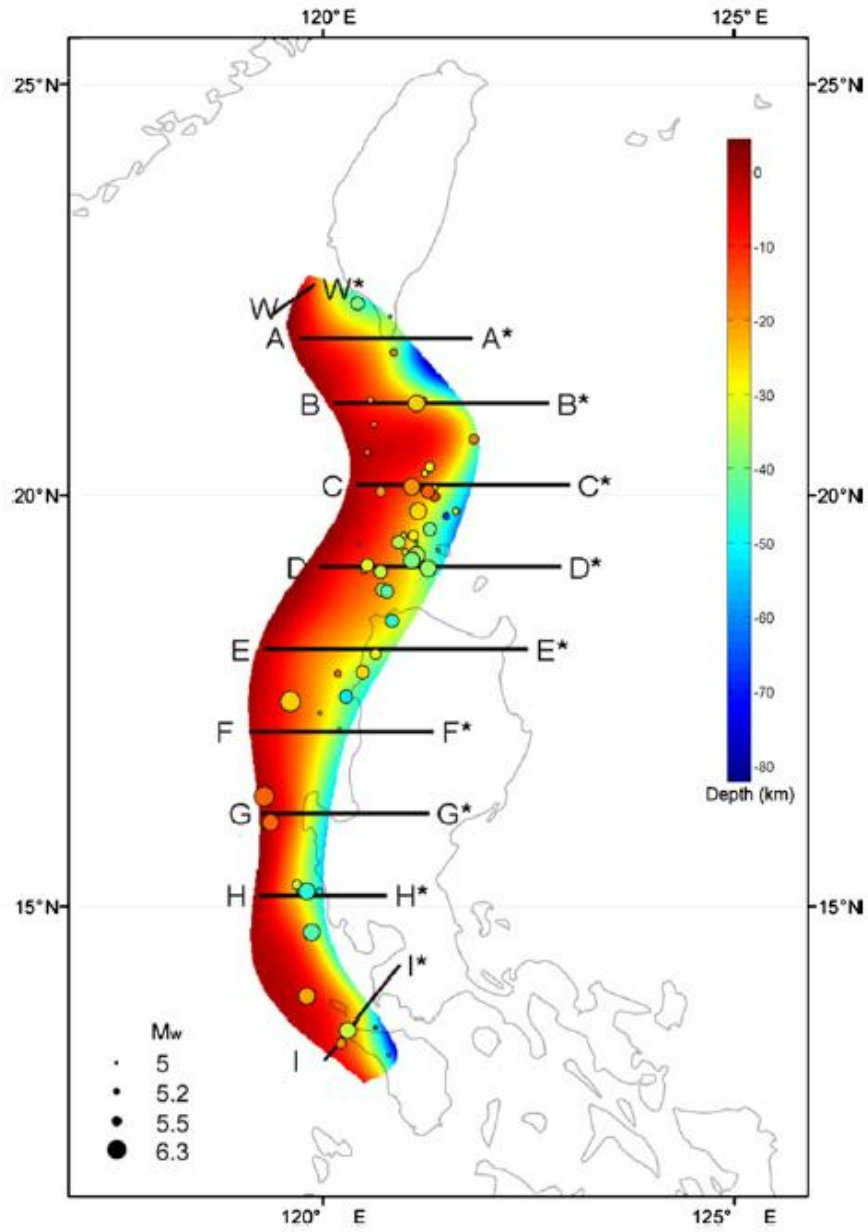


Figure 2

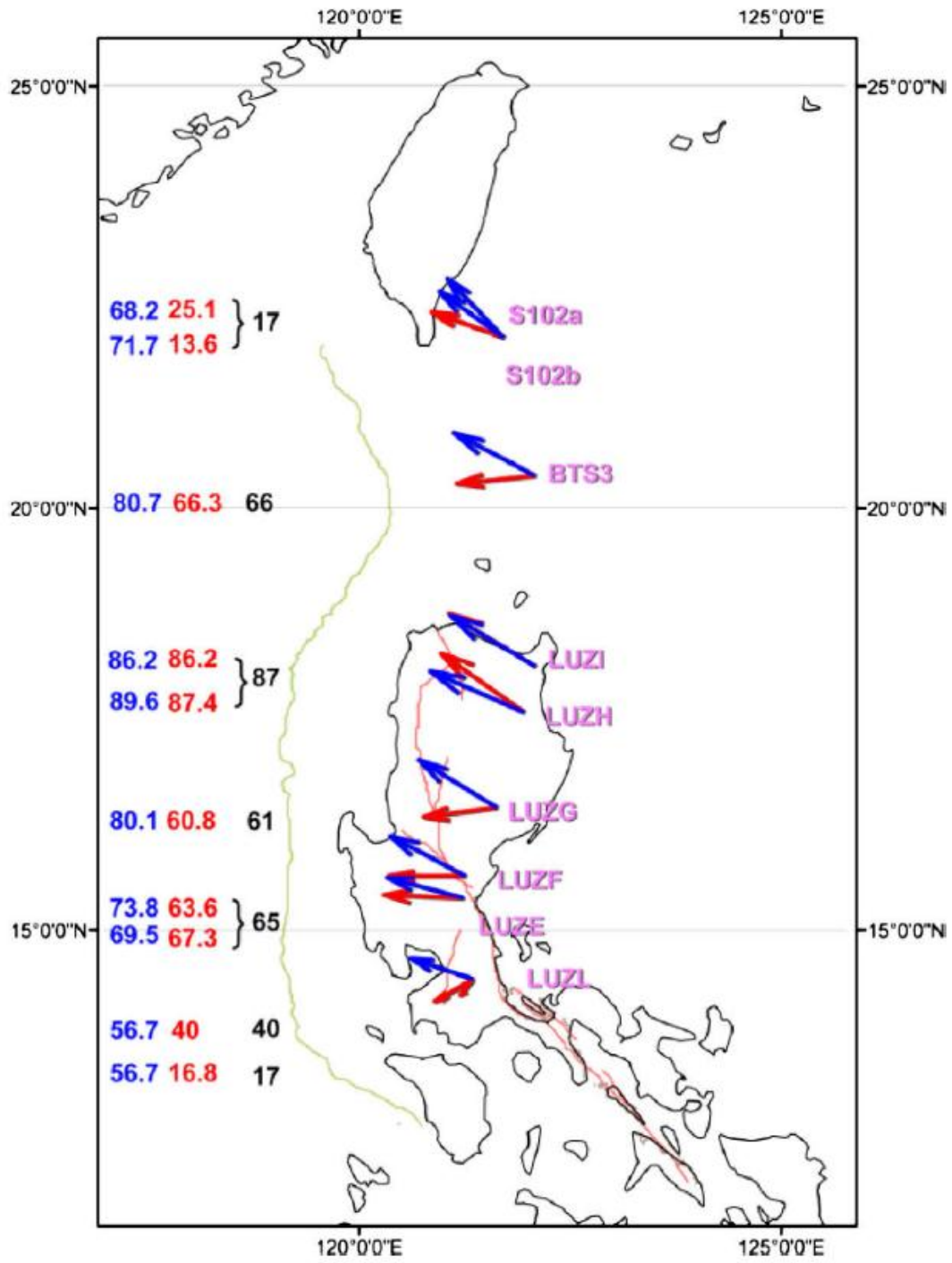


Figure 3

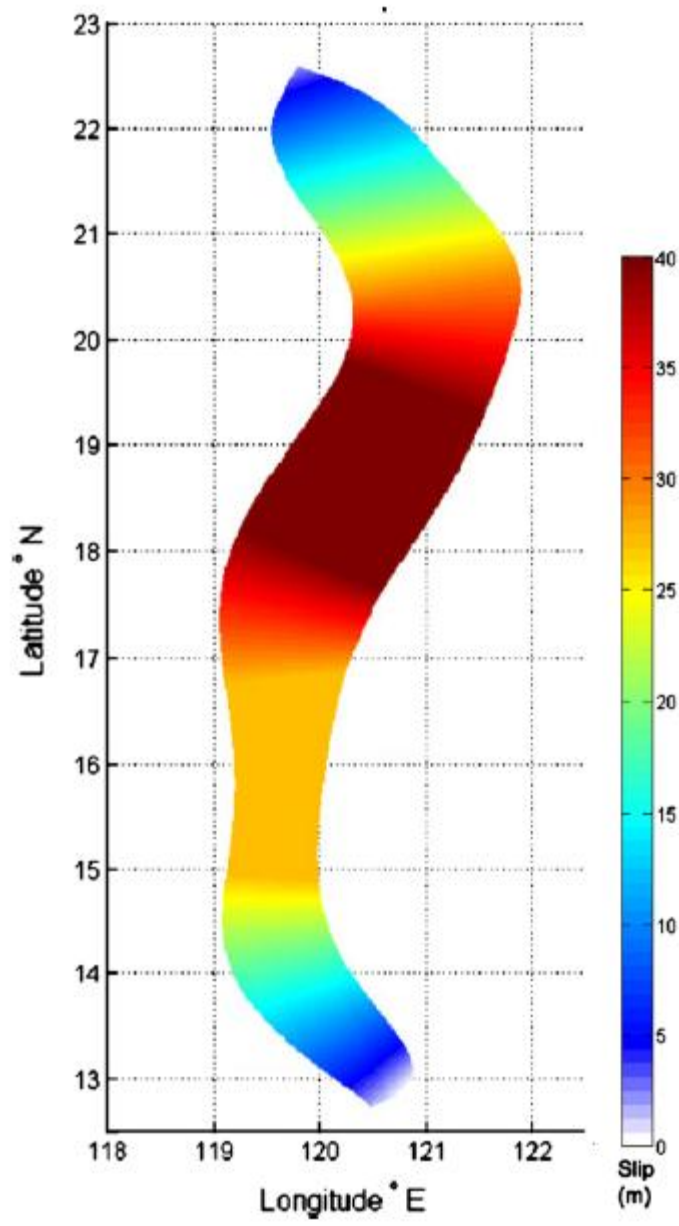


Figure 4

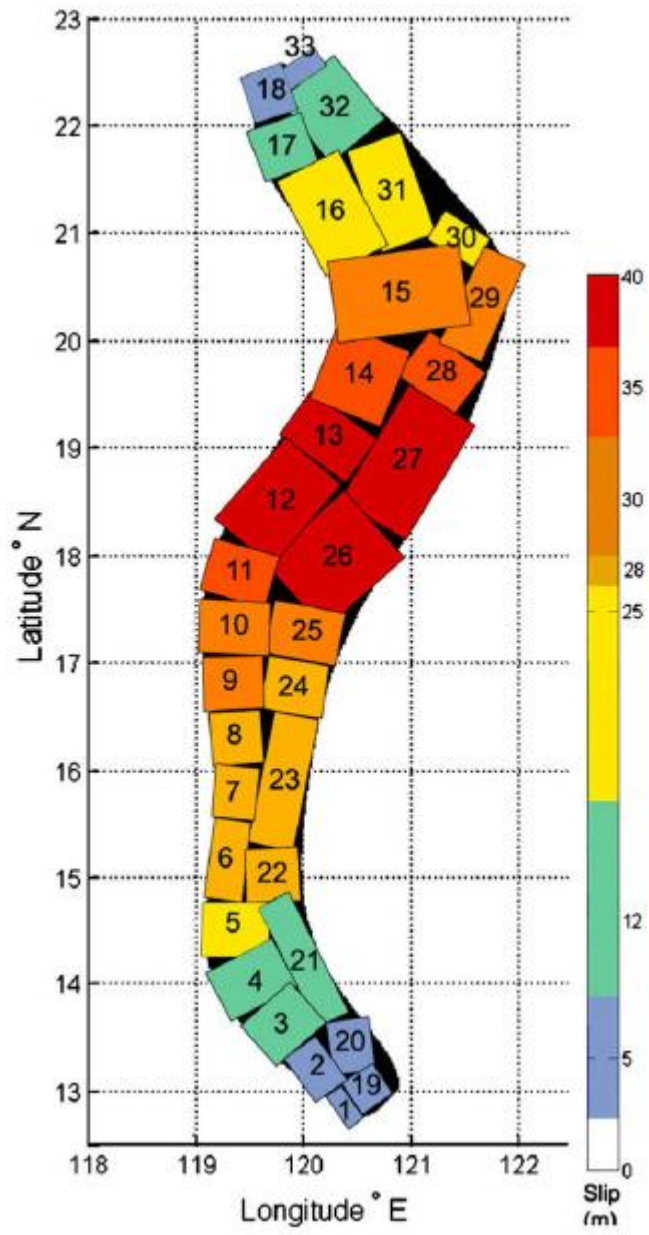


Figure 5

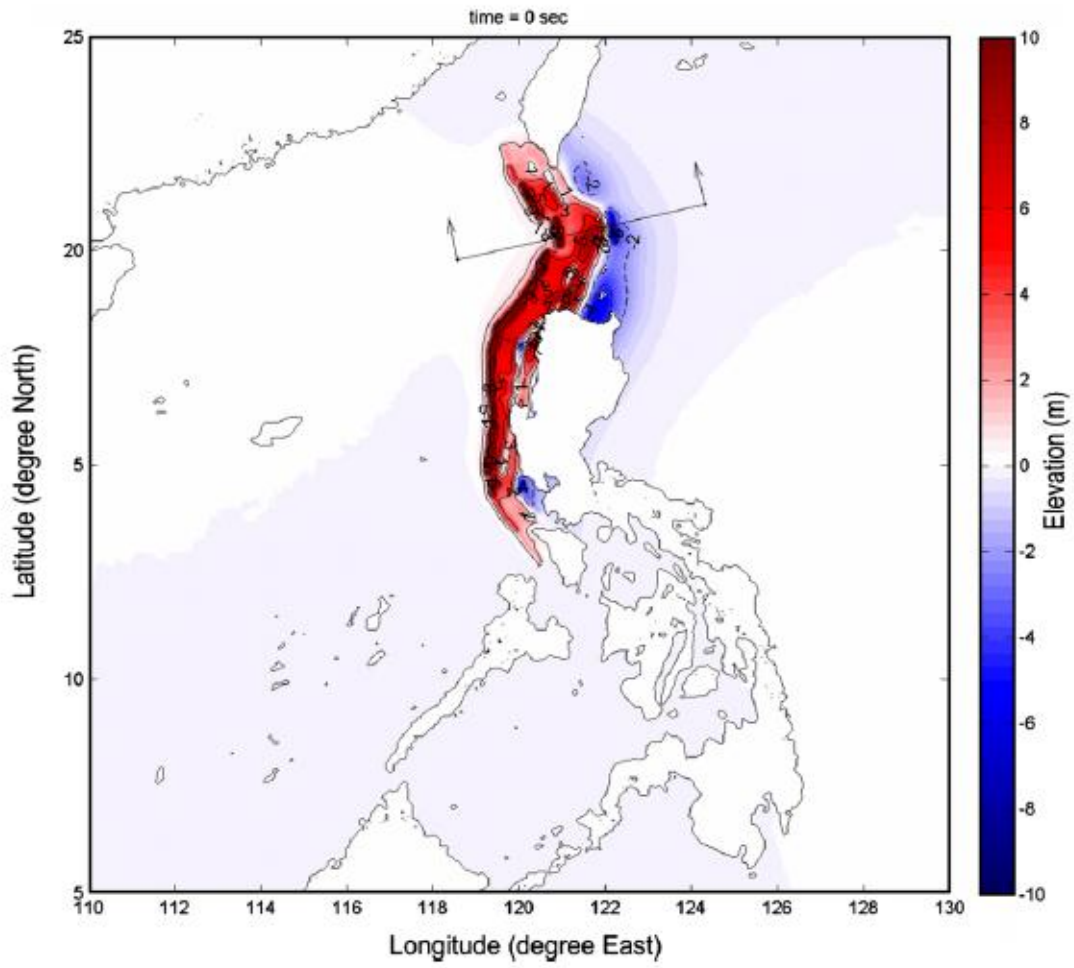


Figure 6

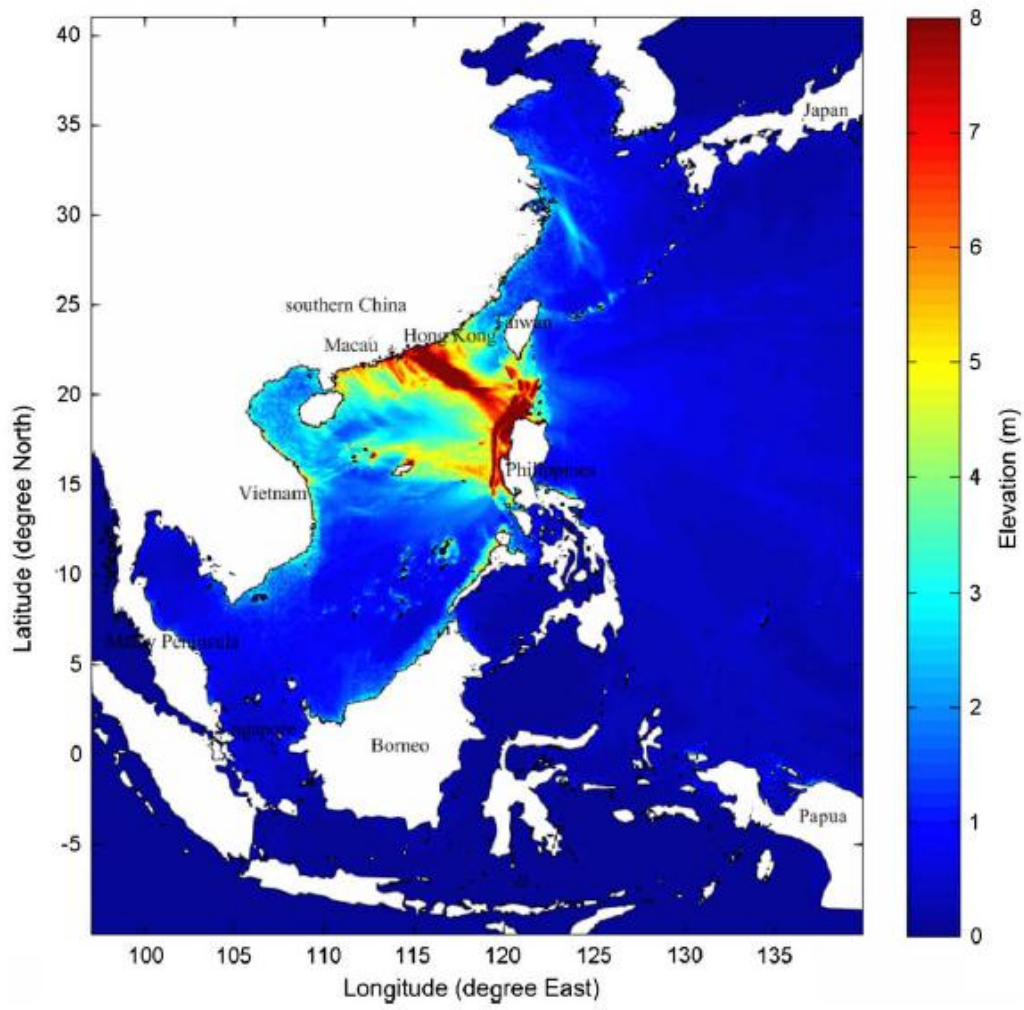


Figure 7